

Performance-based seismic design via Yield Frequency Spectra^{*}

Dimitrios Vamvatsikos^{1,†,‡}, and Mark A. Aschheim²

¹ *Assistant Professor, School of Civil Engineering, National Technical University of Athens, Greece*

² *Professor, Department of Civil Engineering, Santa Clara University, CA*

SUMMARY

Yield Frequency Spectra (YFS) are introduced to enable the direct design of a structure subject to a set of seismic performance objectives. YFS offer a unique view of the entire solution space for structural performance. This is portrayed in terms of the mean annual frequency (MAF) of exceeding arbitrary ductility (or displacement) thresholds, versus the base shear strength of a structural system having specified yield displacement and capacity curve shape. YFS can be computed nearly instantaneously using publicly available software or closed-form solutions, for any system whose response can be satisfactorily approximated by an equivalent nonlinear single-degree-of-freedom oscillator. Because the yield displacement typically is a more stable parameter for performance-based seismic design compared to the period, the YFS format is especially useful for design. Performance objectives stated in terms of the MAF of exceeding specified ductility (or displacement) thresholds are used to determine the lateral strength that governs the design of the structure. Both aleatory and epistemic uncertainties are considered, the latter at user-selected confidence levels that can inject the desired conservatism in protecting against different failure modes. Near-optimal values of design parameters can be determined in many cases in a single step.

KEY WORDS: performance-based seismic design; nonlinear analysis; uncertainty; hazard; confidence; mean annual frequency

1. INTRODUCTION

The need for performance-based seismic design (PBSD) became evident following large economic losses in the 1994 Northridge and 1995 Hyogo-Ken Nambu Earthquakes. Rather than focusing solely on life-safety performance, PBSD targets multiple performance objectives, each typically defined as not exceeding a prescribed structural response level with

^{*} Based on a short paper presented at the at the Vienna Congress on Recent Advances in Earthquake Engineering and Structural Dynamics, Vienna, Austria, 2013.

[†] Correspondence to: Dimitrios Vamvatsikos, National Technical University of Athens, 9 Heroon Polytechniou, Athens 15780, Greece.

[‡] E-mail: divamva@mail.ntua.gr

a mean annual frequency higher than specified. At its most advanced form, specific non-exceedance rates of economic losses or casualties can be targeted, echoing the definition of decision variables that is embedded in the Cornell-Krawinkler framework [1], adopted by the Pacific Earthquake Engineering Research (PEER) Center.

Despite the apparent value of PBS, progress in developing a practicable design process has been slow. This comes as no surprise as design for specified performance is an inverse problem. Since the functional relationship between the design variables and the performance objectives is not invertible, design iterations are necessary. Each iteration requires a costly cycle of re-design and re-analysis, where the latter is a full-blown performance-based assessment involving nonlinear static or dynamic runs. Thus, attempts to represent PBS often have focused on assessment instead (e.g. fib [2], FEMA-445 [3]). Any method built on this paradigm, conceptually framed by Krawinkler et al. [4], essentially is an iterated assessment procedure. Many researchers have chosen to improve the efficiency of re-design to hasten convergence. For example, the use of numerical optimization has been suggested by Mackie and Stojadinovic [5] for bridges and by Fragiadakis and Papadrakakis [6], Franchin and Pinto [7] and Lazar and Dolsek [8] for reinforced-concrete buildings (see Fragiadakis and Lagaros [9] for a comprehensive review). Clearly, the implementation of such PBS approaches is not trivial.

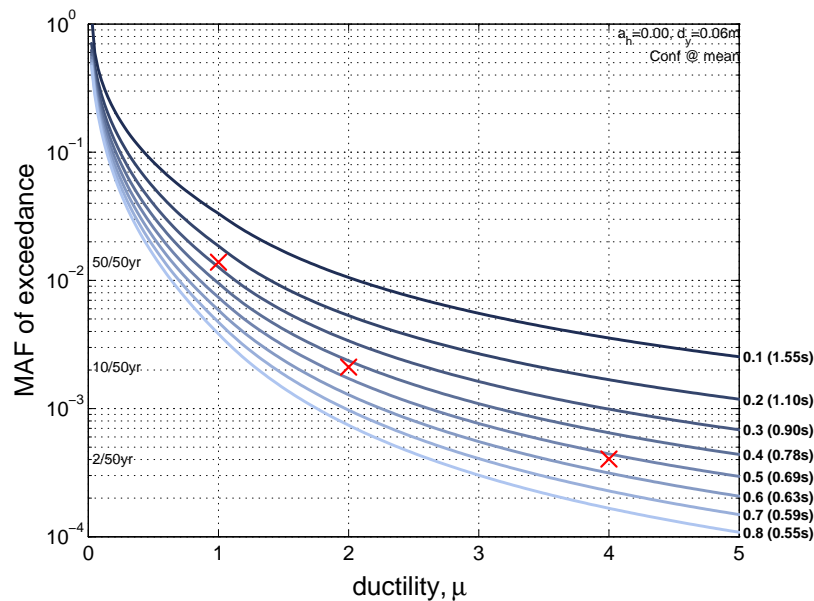


Figure 1. Yield Frequency Spectra showing contours for $C_y = 0.1, 0.2, \dots, 0.8$ determined for an elastoplastic system ($\delta_y = 0.06\text{m}$, $\zeta = 5\%$) at a high-seismicity site. “X” symbols represent discrete performance objectives ($\mu = 1, 2$, and 4 at 50% , 10% and 2% in 50yrs exceedance rates, respectively). The largest of the C_y values associated with each performance objective ($C_y = 0.53$) governs the design; the corresponding period is $T = 0.68\text{s}$.

As an alternative, so-called “Yield Frequency Spectra” (YFS) are proposed as a design aid, being a direct visual representation of a system’s performance that quantitatively links the mean annual frequency (MAF) of exceeding any displacement value (normalized by its yield value to become ductility μ) with the system yield strength (normalized by the seismic weight W to become the yield strength coefficient C_y). YFS are plotted for a specified system yield displacement; consequently, variations in strength (C_y) shown on a YFS plot are associated with variations in stiffness and period of vibration, T . Figure 1 presents a YFS plot for an

elastic-perfectly-plastic oscillator. Three performance objectives are specified (the “x” symbols) while curves representing the site hazard convolved with system fragility are plotted for fixed C_y values. The performance objectives occupy fixed positions on the plot, while the constant strength contours vary with site hazard, yield displacement, and system characteristic hysteretic behavior. Of course, increases in C_y reduce the MAF of exceeding a given ductility value (except for the relatively rare case of inversion, described later). Thus, the minimum acceptable C_y (within some tolerance) that fulfils the specified set of performance objectives can be determined for the site hazard, for a given single-degree-of-freedom (SDOF) system having a particular hysteretic behavior. This strength can be used as a starting point for the PBSO of more complex structures, potentially offering a viable solution in a single step, given a good estimate of the yield displacement.

A key notion (as advocated by Priestley [10], Aschheim [11], Priestley et al. [12]) is that the yield displacement of a bilinear approximation to the first mode pushover curve is stable with changes in strength. In routine design, the overall geometry of the structure is known (e.g. beam spans and story heights) along with the materials of construction. Changes in lateral strength typically are achieved not by changing material properties but by changing the amount of material present (e.g. weight of steel shapes, amount of reinforcement in reinforced concrete members), which causes changes in stiffness and in the period of vibration (e.g. Figure 2). Hence, the yield displacement is largely determined by kinematics and changes little with system strength. In other words, design for multiple performance objectives may proceed based on an estimate of the yield displacement, while the period is determined from the strength required to satisfy the governing performance objective, rather than being estimated at the start of the process. As a result, numerous iterations on period can be avoided.

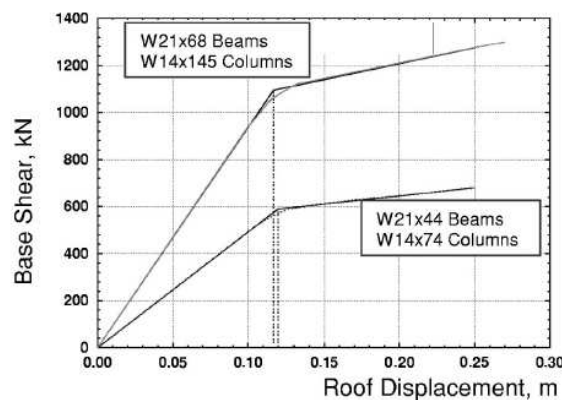


Figure 2. Capacity curves determined by first mode nonlinear static (pushover) analysis of two four-story moment-resisting steel frames. The frames have the same story heights and nominal section depths. Even as the weights of steel sections were changed to affect significant changes in lateral strength, the yield displacement (of a bilinear curve fitted to the capacity curves) remained nearly constant (from Aschheim and Black [13]).

2. BASIS OF DESIGN

2.1. Probabilistic framework

A comprehensive site hazard representation that is compatible with current design norms is provided by the seismic hazard surface, a 3D plot of the MAF of exceeding any level of the intensity measure (IM), typically the elastic spectral acceleration $S_a(T, \zeta)$ for damping $\zeta = 5\%$,

spanning the full practical range of periods (Figure 3). This is the true representation of the expected seismic loading (formally, the mean estimate considering epistemic uncertainty) for any given site. More familiar 2D plots can be produced by taking a cross-section (or contours) of the hazard surface. Cutting horizontally at given values of MAF produces the corresponding uniform hazard spectra (UHS). For example, at a MAF of $P_o = -\ln(1-0.10)/50 = 0.0021$ per year, or a 10% in 50yrs probability of exceedance (Figure 4a), one obtains the spectrum typically associated with design at the ultimate limit-state (commonly referred to as the Life Safety level). Taking a cross-section at a given period, T , produces the corresponding $S_a(T, \xi)$ hazard curve (Figure 4b). In other words, an iso- P_o contour of the hazard surface is the UHS at the given P_o , while an iso- T contour is the S_a hazard curve for the given T .

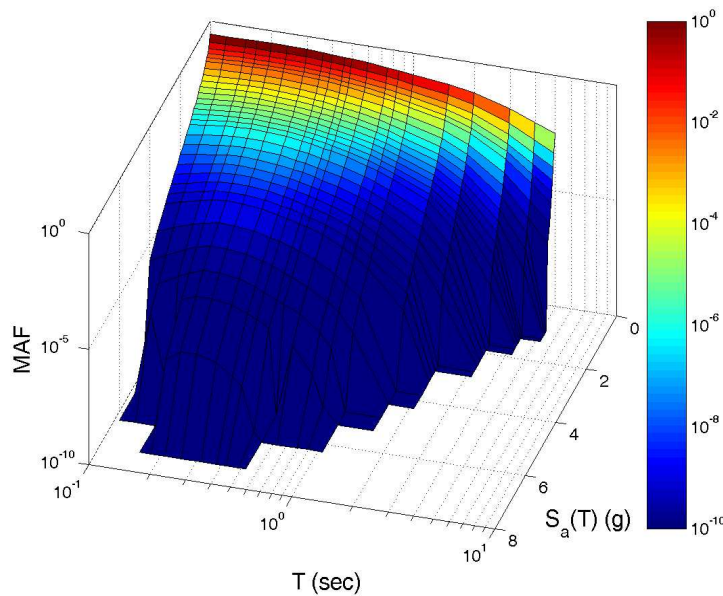


Figure 3. Spectral acceleration hazard surface for a high-seismicity site.

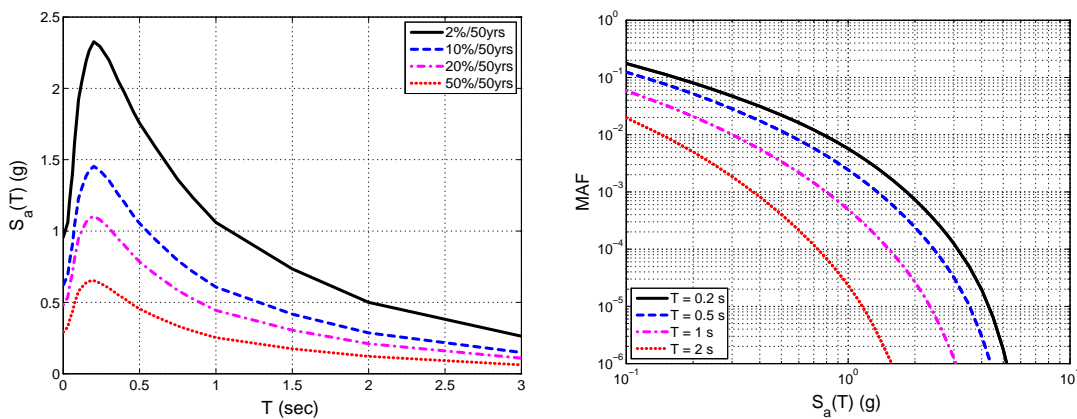


Figure 4. (a) Uniform hazard S_a spectra and (b) S_a hazard curves from the hazard surface of Figure 3.

For realistic inelastic systems, the true nonlinear and uncertain relationship of IM and response, represented by an engineering demand parameter (EDP) considerably complicates design. Nonlinearity in response breaks the analytical relationship between strength (or S_a) and displacement (or spectral displacement S_d) that holds for the response of linear SDOF systems to ground shaking. The nonlinear relationship is conveniently represented by incremental dynamic analysis (IDA, [14]) curves, whose intricate behavior under different

ground motion records and levels of the IM appears in Figure 5 for a nonlinear SDOF system. As shown by Cornell et al. [15], the dispersion around the IM–EDP relationship, e.g., due to higher modes or uncertainty, means that other hazard levels in addition to P_o need to be considered. IM values lower than the one corresponding to P_o appear much more frequently (i.e., having a higher hazard rate in Figure 4b), while, thanks to the associated EDP dispersion, they are still capable of producing higher response than δ_{lim} . Thus, the transformation from the MAF of the IM to that of the EDP is represented by an integral [16,17]:

$$\begin{aligned} \lambda(\delta) &= \int_0^{+\infty} F(S_{ac}(\delta) | s) |dH(s)| \\ &= \int_0^{+\infty} F(S_{ac}(\delta) | s) \left| \frac{dH(s)}{ds} \right| ds, \\ &= \int_0^{+\infty} f(S_{ac}(\delta) | s) \cdot H(s) ds \end{aligned} \tag{1}$$

where $\lambda(\delta)$ is the MAF of exceeding δ ; $S_{ac}(\delta)$ is the (random) limit-state capacity, representing the minimum IM level for a ground motion record to cause a displacement of δ (see Figure 5); $F(\cdot)$ is the cumulative distribution function (CDF) of S_{ac} evaluated at a spectral acceleration value of s ; $f(\cdot)$ is the probability density function (PDF), and $H(s)$ is the associated MAF of the IM. The absolute value is needed for the differential of $H(s)$ because the hazard is monotonically decreasing, thus having a negative slope (and differential).

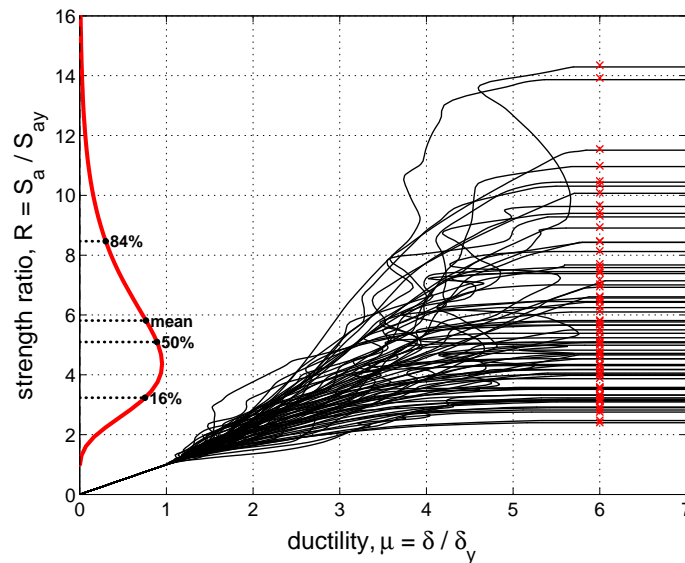


Figure 5. IDA curves for a $T = 1$ s oscillator with a trilinear capacity curve having initially positive and then negative post-yield stiffness. Along the vertical axis, the distribution of spectral acceleration capacity, S_{ac} (normalized by the yield spectral acceleration, S_{ay}) is shown, corresponding to the collapse ductility of $\mu = 6$.

2.2. Code-compatible versus performance-based design

Equation (1) embodies a fundamental difference between conventional and performance-based design. In terms of assessment, it implies that the MAF associated with a given level of

IM is not the same as the MAF of the EDP response that would (on average) correspond to this IM. In other words, checking probability at the input level of the IM is not the same as checking it at the output EDP. In short, conventional, code-compatible (force-based) design, as well as current displacement-based design procedures (e.g. Priestley et al. [12]), rely on the first approach; PBSD methods embrace the second.

In specific, the PBSD of an inelastic system, e.g., an SDOF system, requires that we estimate the yield strength, $F_y = C_y \cdot W$, and period T for which a limiting displacement, δ_{lim} , is exceeded at a rate lower than a given P_o , a requirement essentially consistent with inverting Equation (1). Seismic design provisions avoid such complexity by implicitly adopting two assumptions: (a) using the strength reduction factor, R , or behavior factor, q , to account for the effect of yielding and ductility on the mean response, (b) ignoring the effect of dispersion in demand or capacity, thus assuming that the seismic loads consistent with P_o correspond to a similar (or lower) rate of non-exceedance of δ_{lim} . These simplifications may cause $\lambda(\delta_{lim})$ to exceed the P_o used for specifying the design spectra. In compensation, additional approximations are used that may introduce a degree of conservatism, such as the establishment of the values of R (or q) (e.g., FEMA P-695 [18]). In the end, one is left uncertain as to the degree of confidence of having achieved the stated objective(s) for any design. As such design provisions are applied to a wide variety of buildings and sites, the margin of safety varies with site and system characteristics, sometimes leading to underperforming structures and other times to costlier than necessary designs. Such criticisms are well known, and provide support for the philosophy of PBSD.

The implications of PBSD can be understood by considering a conceptual application within a code-based format: The design of a first-mode dominated structure, for which a basic elastic-static analysis is acceptable. If the smoothed code spectrum is replaced by the more accurate UHS of Figure 4a, then, for any given performance objective P_o (e.g., 10% in 50yrs) structural design values (or EDPs) are determined by elastic static analysis under the intensity $S_{a,des} = H^{-1}(P_o)/R$; R is the strength reduction factor and $H^{-1}(\cdot)$ the inverse of the hazard function. To avoid short-period displacement amplification issues, the structure is assumed to lie within the equal displacement range (e.g., $T > 0.7$ sec), so that $R = \mu$ (where μ is the global or system ductility). Let θ be the deformation (or displacement) EDP that governs the seismic design and θ_D its elastic-static analysis estimate. For the sake of generality, we consider that the strength of ductile members can be checked in the same way, e.g. replacing the plastic moment strength evaluation by comparing the yield rotation times μ to the rotation capacity at ultimate, while brittle elements can be sized to avoid failure and thus do not enter this exercise. Then, the critical EDP demand is estimated as $R \cdot \theta_D$ and it should not exceed the corresponding capacity θ_C . For simplicity, it is assumed that the ‘‘perfect’’ period T_1 has been established for this structure and any pertinent safety factors are explicitly incorporated in the respective demand and capacity values. The governing safety checking becomes:

$$\theta_D R \leq \theta_C \Rightarrow a S_{a,des} R \leq \theta_C \Rightarrow S_{a,des} R \leq \theta_C / a, \quad (2)$$

where a is a constant factor (for an elastic-static analysis) that maps $S_{a,des}$ to θ (see also Equation (9) later). If the structure is perfectly proportioned, without any overstrength, equality holds in the above expression. Then, by employing a closed-form solution [15] for Equation (1), the MAF of exceeding the EDP limit-state associated with θ_C is

$$\begin{aligned} \lambda_{LS} &= H(\theta_C / a) \cdot \exp(0.5k^2 \beta_{T\theta}^2) = H(S_{a,des} R) \cdot \exp(0.5k^2 \beta_{T\theta}^2) \\ &= H(H^{-1}(P_o)) \cdot \exp(0.5k^2 \beta_{T\theta}^2) = P_o \cdot \exp(0.5k^2 \beta_{T\theta}^2). \end{aligned} \quad (3)$$

$\beta_{T\theta}$ is the overall demand and capacity dispersion, and k is the hazard curve log-slope.

Thus, the achieved MAF of exceedance is higher (i.e., unsafe) than the prescribed P_o by the exponential term in Equation (3). This is a well-known issue that has been discussed at least by Cornell et al. [15] and Bradley [19] from the viewpoint of assessment. For a serviceability limit-state, typical values of $k = 1.5 - 3$ (higher values in higher seismicity areas) and $\beta_{T\theta} \approx 0.2$ would result in a bias factor of 1.05 to 1.2 (the exponential term). This level of unconservatism likely is small enough to be mitigated by inherent overstrength. For ultimate limit-state checking though, one may expect $k = 2 - 4$ and $\beta_{T\theta} \approx 0.4$. Then, our example code-based design would have a MAF that is 1.4 – 3.6 times the target P_o . Whether available overstrength can reduce this amplification to an acceptable value is unclear. As Equation (3) shows, relying on such coarse measures to counter the problems inherent in the code does not assure consistent results: k depends on the site hazard, while $\beta_{T\theta}$ varies with period, R , epistemic uncertainties associated with the structural model, the limit-state being checked, and the analysis method used. Thus, a rational safety factor depends on all such properties, a concept that is embodied in the code-compatible safety factors suggested by Cornell et al [15] and Vamvatsikos [20]. If we employ PBSO, the yield strength coefficient C_y is directly provided by inverting a (more accurate) form of Equation (3) for $\lambda_{LS} = P_o$. If the estimate of the yield displacement is correct and the structure is again perfectly proportioned, it will achieve by definition a perfect MAF of $\lambda_{LS} = P_o$.

3. SEISMIC DESIGN VIA YFS

In the following, we offer a practicable, theoretically consistent procedure that can successfully address the inelastic single- and multi-degree-of-freedom (MDOF) design problem. Input data necessary to apply this approach are (a) the site hazard, (b) an assumption about the system's damping, force–deformation characteristics and hysteretic behavior (e.g., 5% damped, bilinear elastic–plastic with kinematic hardening hysteresis), (c) the general dimensions and mass distribution of the structure, and (d) a set of performance objectives comprising values of limiting ductility and the corresponding allowable MAFs of exceedance. In a graphical format, the proposed solution is represented using YFS (Figure 1).

3.1. Definition of YFS for SDOF systems

The peak response of an elastic SDOF system is directly related to the site hazard via S_a hazard curves (Figure 4b). Their direct equivalents for a yielding SDOF system are inelastic displacement (or drift) hazard curves. These are determined by using Equation (1) to estimate the MAF of exceeding any limiting value of (inelastic) displacement. They have appeared at least in the work of Inoue and Cornell [21] and subsequently discussed further by Bazzurro and Cornell [22] and Jalayer [16]. While useful for assessing the performance of a given structure, they lack the necessary generality to enable its design. An appropriate normalization may be achieved for an oscillator having yield strength F_y , and yield displacement δ_y , by using ductility $\mu = \delta / \delta_y$, in place of displacement δ , and using the yield strength coefficient $C_y = F_y / W$ instead of F_y , where W is the seismic or reactive weight. For SDOF systems, C_y is numerically equivalent to $S_{ay}(T, \zeta) / g$, i.e., the spectral acceleration value to cause yield in units of g , at the period T and viscous damping ratio ζ of the system.

Similar plots of SDOF peak inelastic displacement hazard curves were presented by Ruiz-Garcia and Miranda [23] using T and C_y as independent parameters. What makes YFS distinct is the use of a specified value of δ_y , which is considered as a nearly invariant parameter in the

design of a given structural system [10,11], to tie together T and C_y . Thus, in YFS, demand curves are plotted for fixed values of C_y , which may be regarded as a surrogate for period, T :

$$T = 2\pi \sqrt{\frac{\delta_y}{C_y g}}, \quad \text{or} \quad C_y = \frac{\delta_y}{g} \left(\frac{2\pi}{T} \right)^2, \quad (4)$$

For a given site hazard, system damping, δ_y , value of C_y (or period), and capacity curve *shape* (as normalized in terms of $R = F/F_y$ and μ), a unique representation of the system's probabilistic response may be gained through the corresponding displacement (or ductility) hazard curve produced via Equation (1). Damping, δ_y , the capacity curve shape and cyclic behaviour (modified as needed to account for P-Delta) are considered as stable system characteristics, which we refer to in a generalized (non-dimensional) sense as "characteristic hysteretic behavior." By plotting such curves of $\lambda(\mu)$ for a range of constant C_y values, we obtain iso- C_y contours of the ductility hazard surface. These contours allow the direct evaluation of system strength and period—i.e., the C_y required to satisfy any combination of performance objectives defined as $P_o = \lambda(\mu_{lim})$, where each limiting value of ductility μ_{lim} is associated with a MAF of exceedance P_o , as shown in Figure 1.

At a certain level, YFS can be considered as a building- and user-specific extension of concepts behind the IBC 2012 [24] risk-targeted design spectra. Whereas the latter are meant to offer a uniform measure of safety, they only do so for one limit-state (global collapse), one target probability level (1% in 50 years), and a single, assumed fragility applied to all lateral-load resisting systems. In contrast, YFS can target any number of concurrent limit-states, each for a user-defined level of performance (or safety), and implicitly employ building-specific fragility functions, through the specification of system characteristic hysteretic behavior.

3.2. Application to MDOF systems

While YFS directly solve the PBSO problem of an SDOF system, application to an MDOF structure will always involve some degree of iteration. To dampen this, we have reformulated the design process to focus on parameters that can be easily estimated prior to detailed structural design and which remain fairly stable as the design progresses. First, as discussed earlier, we make use of the stability of the yield displacement. Second, similar to all code approaches, we base the design of the multi-degree of freedom system on the use of a so-called "equivalent" SDOF (ESDOF) system. We use this approximation to determine the base shear strength required to limit system level displacement (and ductility) responses to acceptable values. Third, as conventionally done, we use initial estimates of modal parameters (first-mode participation factor, Γ_1 , first mode mass participation factor, α_1 , and coefficient of distortion, α_{COD}) derived for assumed mass distributions and first mode shapes, and update their values in subsequent design iterations, where needed.

As a result of such assumptions, some inaccuracies are to be expected. First of all, due to the ESDOF approximation, performance objectives tied to response quantities that correlate well with SDOF response will be easily met. More localized responses and those significantly affected by higher modes will be addressed less accurately, and therefore, additional analysis and refinement of the preliminary design may be necessary. Then, there is the implicit assumption that $S_a(T_1, \zeta)$ is a sufficient IM to allow the accurate estimation of performance via Equation (1). As reported in recent literature this is not always the case (e.g. [25]). A pertinent spectral shape correction factor has been offered by Haselton et al. [26] and carried forward into FEMA P-695 [18], yet it does not fully resolve sufficiency, as it has been derived only for collapse and a single set of ground motions. Finally, as discussed in a later section, the

rapid estimation of YFS relies on the use of regression expressions. These are the so-called R - μ - T relationships generally connecting the statistics of reduction factor R and ductility μ (with the inelastic displacement ratio $C = \mu/R$ sometimes replacing one of the two) for a given period and characteristic hysteretic behavior (Miranda [27]). These inherently constrain the accuracy of the design C_y when based on ground motions or hysteretic behavior that are not representative of site characteristics (due to soft soil, directivity etc.) or structural properties, respectively. Obviously, all of the above issues are present in standard code approaches as well; yet they are by no means insignificant and should not be discounted.

As appropriate to a bona fide PBSB approach, sources of uncertainty are best addressed explicitly when determining YFS. Assuming that no bias is introduced by uncertainty, Cornell et al. [15] suggest the use of MAF estimates corresponding to specific confidence levels to introduce a desired level of safety. Thus, each response quantity (demand) and its associated limiting value (capacity) are considered to be lognormally distributed random variables that, in addition to any aleatory randomness (e.g., due to record-to-record variability for responses), may also incorporate additional epistemic uncertainty that is assumed to increase their dispersion without changing their central value (e.g., mean or median). Then, an appropriate level of confidence, e.g., $x = 70\%$ to 95% , is chosen for use in design, considering the consequence (e.g., mode of failure) that would result if the EDP capacity should be exceeded. By specifying x together with the appropriate dispersions, additional safety is supplied to ensure that the requested check is satisfied $x\%$ of the time in the presence of uncertainty. This is the approach employed in [28], using confidence as a tunable safety factor to deliver the required level of protection for each mode of failure. Of course, the assumption that EDPs conform to parametric distributions (typically lognormal) is made for numerical convenience but is not an essential feature of using YFS.

In the end, although design according to YFS can eliminate many cycles of iteration (owing to the stability of the yield displacement) while also accounting explicitly for uncertainty and simultaneously addressing multiple performance objectives, the resulting initial design will not necessarily be perfectly compliant. Some re-analysis and re-design iterations may be required, but the initial design based on YFS will provide a good starting point, just as a better initial guess will improve the convergence of any iterative method (e.g., Newton-Raphson). Therefore, if strict compliance to the stated performance objectives is desired, YFS design should be followed by a proper performance assessment, not unlike what is required in other PBSB methods [4, 9]. In more routine cases, the initial design may be deemed adequate, just as designs based on current code requirements are judged acceptable on the basis of equivalent static analysis.

3.3. YFS curve characteristics

YFS are essentially iso-period or iso-strength contours associated with the MAF of exceedance of system peak displacement (or ductility). They are much like the contours of Figure 4b relative to the hazard surface of Figure 3, only determined by a different process and for an inelastic system. In general, their shape conforms to the characteristics displayed in Figure 6a, showing two distinct monotonicity properties, both involving a rapid decrease of MAF with (a) increasing ductility and (b) increasing strength (or decreasing period). Yet, both may be partially violated under specific conditions (Figures 6a, 7a, 7b).

Strict monotonicity with ductility is violated when an ultimate ductility is introduced in the supplied characteristic hysteretic behavior. In this case, YFS will display a “flatlining” (Figure 6b, see also Jalayer [16]). This phenomenon correlates to the flatlining observed in

IDA curves as in Figure 5, where dynamic instability appears as a rapid (infinite) increase in response amplitude for small changes in the intensity [14]. In contrast to the unbounded nature of both IDA curves and YFS for unlimited ductility systems (Figure 6a), dynamic instability enforces a lower bound on the potential MAF values, essentially stating that the lowest achievable system MAF is the one of collapse. Thus, it would be more general to say that YFS are non-increasing (rather than strictly decreasing) with ductility.

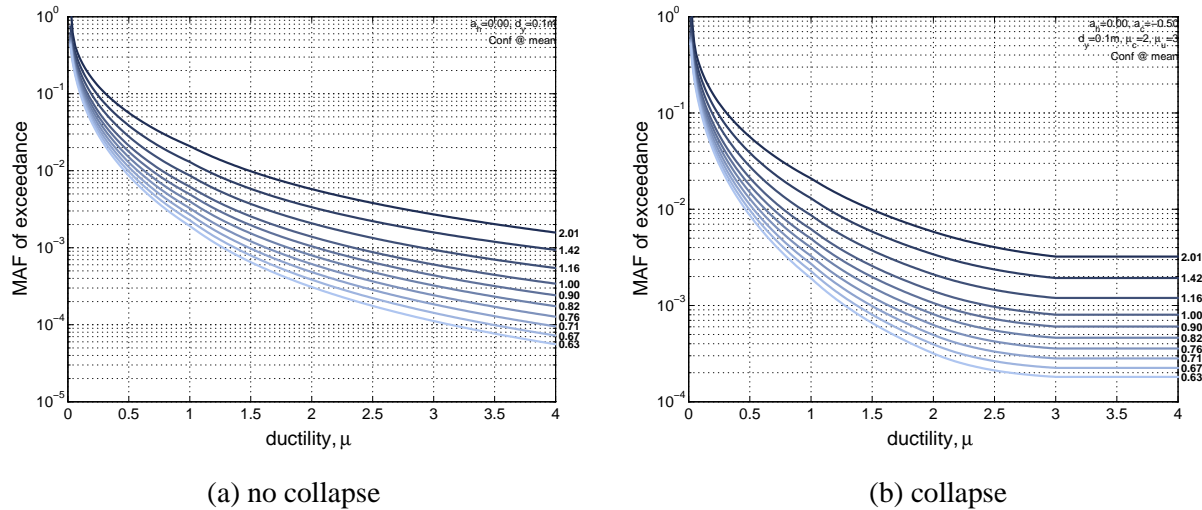


Figure 6. YFS created for (a) an elastoplastic system, (b) an elastic-plastic-negative system having an ultimate (collapse) ductility of $\mu_u = 3$, creating the YFS flatlines ($\zeta = 5\%$).

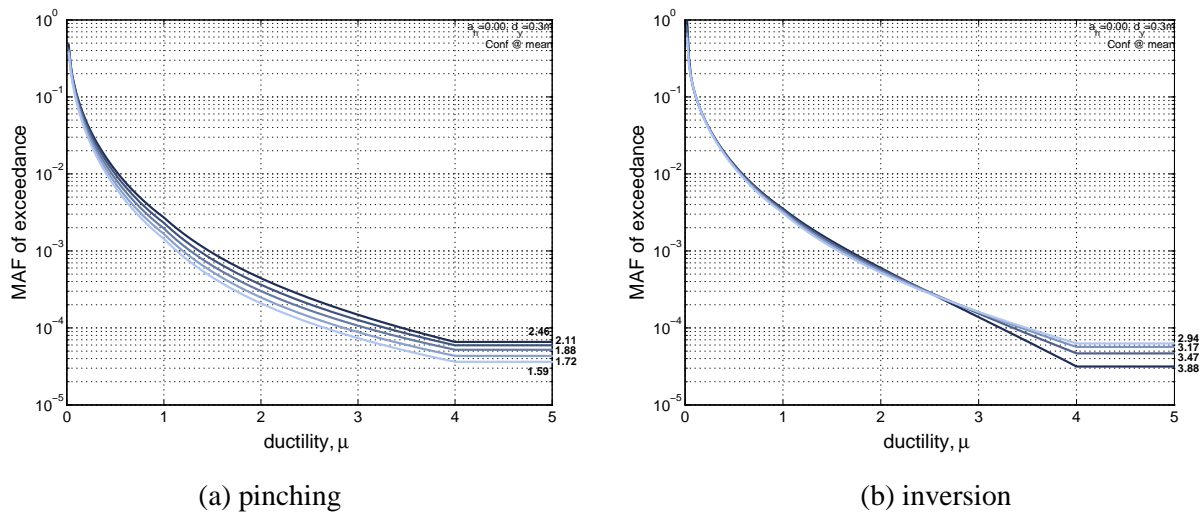


Figure 7. YFS of an elastoplastic system ($\zeta = 5\%$) with an ultimate ductility of $\mu_u = 4$: (a) Long periods in the equal elastic–inelastic displacement and constant spectral displacement region force the “pinching” of the contours, while (b) even longer periods with $C_\mu < 1$ lead to contour inversion.

YFS monotonicity with strength (or period) may be violated even more severely, similarly to the apparent non-monotonic shape of S_a spectra, where lower periods may or may not have higher accelerations. To understand this, one must consider Equation (1). This is used to generate YFS by the convolution of the S_a -hazard curves with R - μ - T relationships, or equivalently S_a -hazard curves with either C_1 - R - T or C_μ - μ - T relationships, where C_1 and C_μ are the inelastic displacement ratios given R and μ , respectively. In general, whenever such regression expressions have been derived for percentile values (e.g., medians), rather than

means, they can be considered as interchangeable [17, 27, 29]. Still, the C_μ - μ - T formulation can provide additional insight for YFS. Figure 8a shows elastic displacement UHS for the hazard surface of Figure 3. Despite the non-monotonic appearance of the corresponding elastic acceleration UHS of Figure 4a, elastic displacement UHS are increasing with period, at least within the range shown. Figure 8b also shows the shape of C_μ - μ - T relationships estimated [29] for ordinary records, i.e., without directivity or soft-soil issues. The iso-ductile C_μ curves decrease monotonically within the period range of practical interest. Finally, the hazard curves themselves are always decreasing with higher intensities, having rapidly diminishing MAFs (Figure 4b). The shapes of these three contributions in combination result in the period/strength monotonicity of YFS. If any of these general characteristics does not hold, then this strict monotonicity observed, e.g., in Figure 6a may be violated.

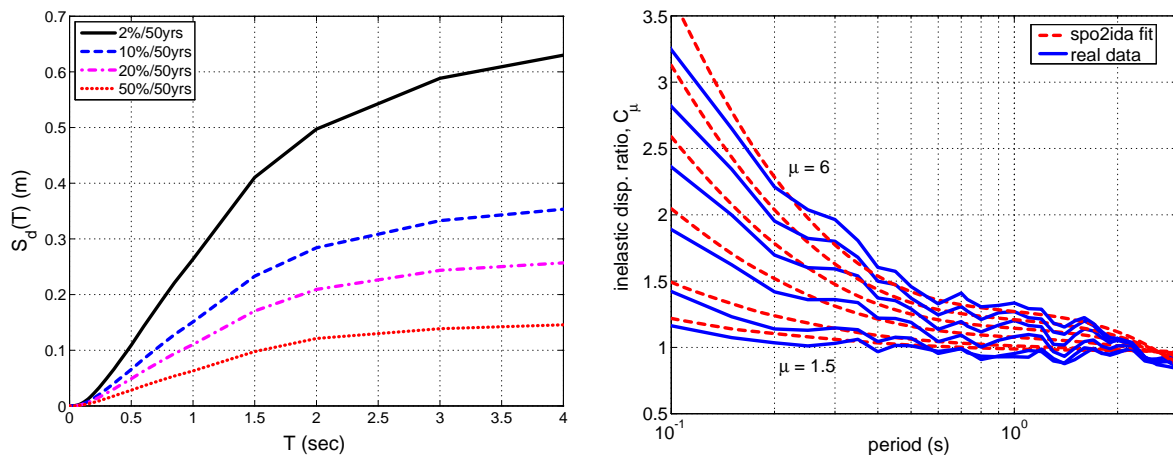


Figure 8. (a) Uniform hazard elastic displacement spectra and (b) fitted versus actual mean inelastic displacement ratio C_μ (adapted from [29]). Values of $C_\mu < 1$ appear for long periods.

At large periods (or low values of C_y), systems having extended non-negative stiffness segments will have a mean C_μ of nearly 1.0 (the equal displacement rule). At the same time the S_d spectra approach their plateau (the constant-displacement region). Thus, multiple values of C_y (or period) can produce similar displacements with the same MAF, causing a characteristic closing (or “pinching”) of the gap between contours (Figure 7a). In some cases, this effect can become strong enough to cause decreasing values of C_y to correspond to *decreasing* values of displacement, essentially inverting the YFS (Figure 7b). This appears, for example, when using actual results from nonlinear dynamic analyses or C_μ - μ - T relationships that do not enforce the equal displacement rule (which is after all just an observation that peak displacements of yielding systems tend to not exceed those of corresponding elastic systems on average, rather than a statement that they are equal). As shown for example in Figure 8b, it is quite possible to have a mean C_μ below 1.0 at longer periods. This could also occur at a soft-soil site, where the C_μ - μ - T relationships differ significantly from the ones shown [30]. Similarly, excessively large periods (typically far larger than 4 sec) will see the displacement spectrum reducing to eventually reach the value of peak ground displacement. Such effects, either isolated or combined, may force a characteristic inversion of the YFS, as shown in Figure 7b, where lower C_y values will be favored for stricter performance requirements (lower MAFs). Such violations of monotonicity are the premise of dynamic loading and should be expected. Nevertheless, they should not pose any problems in practical design as they occur at large periods and intolerably large deformations, where P-Delta effects become important. Unless base isolation is considered,

serviceability requirements will typically control the design in most (if not all) such situations.

4. ESTIMATION OF YFS

The practical estimation of YFS is based on calculating the MAF of exceeding given values of system ductility through the integral of Equation (1). This involves a comprehensive evaluation for a number of SDOF oscillators with the same characteristic hysteretic behaviour but different periods and yield strengths. Two options are offered: a numerical approach and a simple analytical approximation; both are capable of achieving accurate point estimates.

4.1. Numerical approach: Basis

To estimate the YFS one needs to calculate $\lambda(\mu)$ for a range of μ_{lim} and C_y values. By plotting them on a graph and interpolating, any performance objective within the plotted range can be satisfied (Figure 1). Alternatively, for each performance objective, one can estimate only $\lambda(\mu_{lim})$ for a trial value of C_y (or T), calculate an updated value of C_y , and iterate until convergence.

When the distribution of S_a capacity is defined by a (lognormal) distribution, rather than discrete points, Equation (1) is evaluated most efficiently by its third form. This involves the PDF for which an analytical formula is available, needing no differentiation. However, accuracy issues may develop when one encounters non-zero dispersions less than 5% for $S_{ac}(\delta)$, i.e., for the S_a capacity given μ or δ . In this case, smart sampling is needed to ensure sufficient integration points are located within the ‘‘core’’ of the capacity PDF. On the other hand, the first form typically needs twice the number of points plus the numerical evaluation of the CDF, but it remains robust regardless of the dispersion and without needing a careful selection of integration points. Being uniquely suitable for practical application in a spreadsheet, its use is advisable for the evaluation of C_y -contours. This moderate-efficiency high-robustness integration scheme has been captured in the following expression [31]:

$$\lambda(\mu) \cong \sum_{\text{all } s_i} F(S_{ac}(\mu) | s_i) \Delta H(s_i), \quad (5)$$

where s_i are a number of IM values covering the entire hazard curve from the lowest to the highest non-zero MAF values available (at least 50 for reasonable accuracy) and $\Delta H(s_i) = H(s_i) - H(s_{i+1}) > 0$, due to the monotonically decreasing hazard.

There are two points that deserve further clarification in the numerical estimation of YFS. First is the issue of damping. In order to declare that $C_y = S_{ay} / g$, S_a should be established using the same viscous damping ratio ζ as the system. Thus, if the nonlinear system has ζ different from the value used to characterize the seismic hazard curve (typically 5%), S_a should be modified by an appropriate factor [32]. Second is the incorporation of uncertainty. To obtain a value of C_y consistent with the mean estimate of the displacement hazard vis-à-vis epistemic uncertainty, then the mean hazard curve should be employed [15] and the (record-to-record) dispersion of $S_{ac}(\delta)$ estimated from the R - μ - T relationship must be increased. Adopting the typical first-order assumption [15], it is assumed that epistemic uncertainty causes the S_{ac} values of capacity to become lognormally distributed with an unchanged median of \hat{S}_{ac} but increased overall dispersion (standard deviation of the log data) of

$$\beta_{Tsc} = \sqrt{\beta_{USc}^2 + \beta_{Sc}^2}, \quad (6)$$

where β_{Sc} is the aleatory dispersion, incorporating the effect of the natural variability of S_{ac} (its record-to-record component determined in establishing the R - μ - T relationship), and β_{USc} is the S_{ac} dispersion due to uncertainty in displacement demand and capacity. The latter may be approximated as the square-root-sum-of-squares of the corresponding uncertainty dispersions in μ_{lim} and in the system EDP demand itself, namely $\beta_{U\theta c}$ and $\beta_{U\theta d}$, an assumption that (strictly speaking) is less accurate for short periods and close to the dynamic instability region. One potential remedy is the estimation of the local slope b of the mean or median R - μ - T function in log-space (akin to fitting the median IDA of Figure 5 with a power law, see also section 4.3). Then, any dispersion in EDP can be divided by b to be transformed locally to IM terms [15]. Any aleatory variability in the EDP capacity with dispersion $\beta_{\theta c}$ can also be incorporated in the same way into the aleatory dispersion associated with the R - μ - T relationship.

Using the above assumptions, Equation (1) will provide an estimate consistent with confidence somewhat higher than 50%, the exact value depending on the overall dispersion. If an estimate compatible with a specific confidence level x in $[0.5, 1.0)$ is desired instead, then the CDF of S_{ac} should retain its aleatory dispersion but receive a reduced median consistent with a $(100 - x)\%$ percentile of the lognormal uncertainty distribution:

$$\hat{S}_{ac}^x = \hat{S}_{ac} \cdot \exp(-K_x \beta_{USc}), \quad (7)$$

where $K_x = \Phi^{-1}(x)$ is the standard normal variate corresponding to the confidence level x , with $\Phi^{-1}(\cdot)$ being the inverse CDF of the standard normal distribution. For example, to completely ignore epistemic uncertainty, setting $x = 50\%$ results in $K_x = 0$, while for a 90% confidence estimate, $K_x = 1.28$.

4.2. Numerical approach: Algorithms

Accurate estimation of YFS necessitates the determination of the distribution of peak displacement for an SDOF system for a wide range of intensities; essentially, it requires the data supplied by IDA. Given the increasing capabilities of computers, performing such an analysis with automated tools may not be unrealistic. In the meantime, using regressed estimates as a substitute, i.e., R - μ - T relationships, is much preferred. As discussed earlier, C_1 - R - T and C_{μ} - μ - T expressions may also be used, all considered to be equivalent if percentile statistics are provided. Henceforth the term “ R - μ - T ” is used to refer to such regression expressions. Of course, for application with Equation (5), such relationships need to describe both the mean (or median) and the dispersion of the distribution of EDP given IM. Two options are currently available: (a) Expressions by Ruiz-Garcia and Miranda [23] for elastoplastic systems and (b) the SPO2IDA tool by Vamvatsikos and Cornell [29]. The former is the simpler but more limited option. SPO2IDA covers a range of characteristic hysteretic curves that includes bilinear, trilinear, and quadrilinear capacity curves, providing the potential for including negative post-yield stiffness (e.g. due to P-Delta or material degradation) and residual strength (e.g. after brace buckling or infill masonry cracking). Both tools have been derived for far-field, firm soil records; care should be exercised for other conditions.

Two modes of application can be undertaken numerically. For obtaining a comprehensive view of YFS contours (e.g. Figure 1), two nested for-loops suffice:

1. Prescribe a set of N equally-spaced C_y values
2. For each C_y :
3. Determine the period T by Equation (4)
4. Extract the $S_a(T, \zeta)$ hazard curve $H(s)$

5. For each μ -value of interest:
6. Determine median and dispersion of $S_{ac}=R(\mu)C_y$ from $R-\mu-T$
7. Modify median and dispersion of S_{ac} to account for uncertainty and confidence
8. Estimate $\lambda(\mu)$ for the given C_y via Equation (5)
9. End for
10. Plot a continuous curve from the $(\mu, \lambda(\mu))$ points
11. End For

The performance objectives can be plotted as (μ_{lim}, P_o) points on the same figure, while accurate values for the C_y corresponding to each can be estimated by a double interpolation: (a) linearly interpolate the $(\mu, \ln\lambda(\mu))$ points along each iso- C_y contour to find values of $\lambda(\mu_{lim})$ that correspond to each C_y ; and then, (b) linearly interpolate the set of N points of $(C_y, \ln\lambda(\mu_{lim}))$ to find the C_y that corresponds to the value of $\ln P_o$. A spreadsheet implementation of the aforementioned process for generating YFS contours is available on the web [33].

Alternatively, if one requires only the values of C_y that correspond to each performance objective, without need to determine the entire YFS, an iterative search algorithm may be used to determine each pair of (μ_{lim}, P_o) :

1. Select an arbitrary initial period T and estimate a trial value of C_y^{trial} , by Equation (4).
2. Extract the $S_a(T, \xi)$ hazard curve $H(s)$
3. For μ_{lim} , determine median and dispersion of $S_{ac}=R(\mu_{lim})C_y^{trial}$ from $R-\mu-T$
4. Modify median and dispersion of S_{ac} to account for uncertainty and confidence
5. Estimate $\lambda(\mu_{lim})$ for the given C_y^{trial} via Equation (5).
6. If this is the first trial C_y , then $C_y^{new} = C_y^{trial} \cdot (P_o / \lambda(\mu_{lim}))^2$.
Else determine C_y^{new} corresponding to P_o by linearly interpolating (or extrapolating) from the previous $(\ln\lambda(\mu_{lim}), C_y^{trial})$ points.
7. If C_y^{new} differs from the last C_y^{trial} by more than a specified tolerance (say 5%), set C_y^{trial} equal to C_y^{new} , recalculate T for the new C_y^{trial} and go to step 2.

This is a rapidly converging algorithm that can provide a good estimate of the design C_y with 3-5 iterations in most cases. Still, the convergence rate will degrade wherever pinching or inversion of YFS appears. As previously discussed, these cases may appear in the constant displacement spectral region for non-degrading systems, where different values of C_y (or period T) will result in nearly the same peak displacements (for elastic and inelastic systems). In this region, peak displacement is insensitive to C_y , resulting in an infinite number of C_y solutions for the same ductility target, at least for the theoretically pure case. Where this occurs, it is best to stop the algorithm early and select the lowest period (highest C_y , within tolerance) that provides the desired displacement, as this appears to be a more sensible basis for characterizing the design space; of course, most designs will be at smaller periods.

4.3. Analytical approach: Basis

As an alternative to numerical integration, Vamvatsikos [20] has provided an accurate closed-form solution for the MAF of inelastic response that can be inverted analytically. The first step is to fit the hazard curve $H(s)$ for $S_a(T_1, \xi)$ (i.e., transformed to the system's damping value ξ) in the range of interest using a second-order power-law:

$$H(s) \approx k_0 \exp(-k_2 \ln^2 s - k_1 \ln s), \quad (8)$$

with $k_0, k_1 > 0$ and $k_2 \geq 0$. The variable k_2 identifies the (local) curvature of the hazard curve; its use provides a significant improvement in precision over the linear fit used in the original

SAC/FEMA formulation [15]. This improved fitting, despite being “local” in nature, encompasses a large enough range of the hazard to allow back-estimation of values of the IM for a required value of MAF, an operation prone to error when using the original formulation.

The EDP capacity is assumed to be lognormal, with median $\hat{\theta}_c$ and dispersions equal to β_{θ_c} and $\beta_{U\theta_c}$ associated with aleatory and epistemic sources, respectively. The distribution of EDP demand given intensity IM is also assumed lognormal, having constant dispersions equal to β_{θ_d} and $\beta_{U\theta_d}$ regardless of the level of intensity, s , and a conditional median $\hat{\theta}(s)$ that can be fitted to the IM using a power-law

$$\hat{\theta}(s) \approx a \cdot s^b \tag{9}$$

by linear regression in log-log coordinates—in the IDA framework, this can be thought of as an approximation of the median IDA curve. When fitting away from the global instability region, the above expression is accurate enough to allow for a useful approximation of the EDP-capacity required to achieve a specified performance level (i.e., MAF of P_o):

$$\hat{\theta}_c = a \cdot \exp \left[\frac{b}{2k_2} \left(-k_1 + \sqrt{\frac{k_1^2}{\phi'} - \frac{4k_2}{\phi'} \ln \frac{P_o}{k_0 \sqrt{\phi'}}} \right) \right], \tag{10}$$

where

$$\phi' = \frac{1}{1 + 2k_2(\beta_{\theta_d}^2 + \beta_{\alpha_c}^2 + \beta_{U\theta_d}^2 + \beta_{U\alpha_c}^2)/b}. \tag{11}$$

Equation (10) is associated with a mean estimate of the MAF considering both aleatory and epistemic sources of uncertainty. In order to estimate the required EDP capacity at a desired level of confidence while accounting for epistemic uncertainty we may use

$$\hat{\theta}_c = a \cdot \exp \left[K_x \beta_{U\theta} + \frac{b}{2k_2} \left(-k_1 + \sqrt{\frac{k_1^2}{\phi} - \frac{4k_2}{\phi} \left(\ln \frac{P_o}{k_0 \sqrt{\phi}} + \gamma_{\alpha_c} \right) + \frac{4k_2^2}{b^2} K_x^2 \beta_{U\theta}^2} \right) \right], \tag{12}$$

where

$$\phi = \frac{1}{1 + 2k_2(\beta_{\theta_d}^2 + \beta_{\alpha_c}^2)/b}, \tag{13}$$

$$\beta_{U\theta}^2 = \beta_{U\theta_d}^2 + \beta_{U\alpha_c}^2, \tag{14}$$

$$\gamma_{\alpha_c} = k_2 \beta_{U\theta}^2 \frac{\phi}{b} \cdot \frac{(1-2x)^2}{(1-x)^{0.4}}, \quad x \in [0.50, 0.95]. \tag{15}$$

Where point-estimates of C_y values are sought, a few variable replacements are needed. First, let the median EDP capacity $\hat{\theta}_c$ be replaced by the displacement capacity, or limit, δ_{lim} and let $\mu_{lim} = \delta_{lim} / \delta_y$ be the corresponding ductility. Now, Equations (10) and (12) are connected to elastic structural properties via coefficient a of the median IDA curve. Taking Equation (9) to hold in the elastic range as well, the yield point is expressed as:

$$a = \frac{\delta_y}{S_{ay}^b} = \frac{\delta_y}{(C_y \cdot g)^b}, \quad (16)$$

where g is the acceleration of gravity. By introducing Equation (16) into Equations (10) and (12) and performing some algebraic manipulations, the following can be obtained:

$$C_y = \frac{1}{g\mu_{lim}^{1/b}} \cdot \exp \left[\frac{1}{2k_2} \left(-k_1 + \sqrt{\frac{k_1^2}{\phi'} - \frac{4k_2}{\phi'} \ln \frac{P_o}{k_0\sqrt{\phi'}}} \right) \right], \quad (17)$$

$$C_y = \frac{1}{g\mu_{lim}^{1/b}} \cdot \exp \left[\frac{K_x \beta_{U\theta}}{b} + \frac{1}{2k_2} \left(-k_1 + \sqrt{\frac{k_1^2}{\phi} - \frac{4k_2}{\phi} \left(\ln \frac{P_o}{k_0\sqrt{\phi}} + \gamma_{\alpha} \right) + \frac{4k_2^2}{b^2} K_x^2 \beta_{U\theta}^2} \right) \right], \quad (18)$$

where g only serves to make sure that the units come out right—if the hazard curve has been fitted with S_a in units of g , then $g = 1$ should be used.

The above equations are powerful approximations as long as they are used away from the region of global collapse, where the basic assumption of Equation (9) does not hold. In this range of validity they provide useful intuition on the interplay between the core design quantities of C_y , μ_{lim} and P_o . First, note that $b = 1$ in the range where the equal displacement rule holds. Values of $b > 1$ may typically appear only for short period structures or for large displacement values that fall into the negative stiffness region, approaching global dynamic instability. Second, parameters ϕ and ϕ' are always within $[0,1]$, moving towards zero as the curvature of the hazard curve, k_2 , or the dispersion β values increase. Thus, increasing dispersion β , decreasing the performance objective P_o (meaning less frequent failures), decreasing μ_{lim} (i.e., targeting a lower damage level) or seeking higher confidence x , will each raise the value of the required C_y . A more aggressive hazard curve will also achieve the same result, although it may not be as evident analytically.

4.4. Analytical approach: Algorithms

While the application of Equations (17) and (18) may seem straightforward, some iteration may be needed due to the dependence of the hazard curve (and the corresponding fit) on the period. This is practically the same search scheme described for the numerical approach, and would be repeated for each performance objective P_o :

1. Select an initial period T , estimate C_y^{trial} by Equation (4).
2. Extract the $S_a(T, \xi)$ hazard curve, $H(s)$.
3. Estimate k_0 , k_1 , and k_2 to fit $H(s)$ in Equation (8).
4. Use the R - μ - T expressions to estimate $\beta_{\theta d}$ and then b via Equation (9).
5. Estimate C_y^{new} via Equation (17) or Equation (18).
6. If C_y^{new} differs from the last C_y^{trial} by more than the tolerance (say 5%), set C_y^{trial} equal to C_y^{new} , recalculate T for the new C_y^{trial} and go to step 2.

Note that convergence is not influenced by the initial choice of T . Thus, any approximate code formula or a ballpark estimate may be used. Within the range of YFS monotonicity it rarely takes more than 3 iterations for the algorithm to converge to within 5% of the C_y value required for any performance objective. Pinching and inversion of YFS will typically degrade the convergence rate, just as for the numerical approach. The overall estimation error can be expected to reach up to 15% vis-à-vis the more accurate numerical approach due to the

approximations introduced in deriving Equations (17) and (18).

Note that for step 3, the scheme proposed by Vamvatsikos [34] is recommended, as it requires no regression. Instead, a three-point interpolation is performed, which is equivalent to solving a 3x3 linear system. The three points are located on the hazard curve at intensities

$$s_i = s_{p_o} \exp\left(c_i \sqrt{\beta_{\theta d}^2 + \beta_{\theta c}^2 + \beta_{U\theta d}^2 + \beta_{U\theta c}^2} / b\right), \quad (19)$$

where $c_i = 0.0, -1.5, -2.5$. The variable $s_{p_o} = H^1(P_o)$ is the $S_a(T_1)$ value corresponding to performance level P_o on the hazard curve. For step 4, R and μ play the roles of the IM and EDP, respectively. The power-law slope b is estimated through a two-point interpolation in log space on the median (or mean) R - μ - T relationship, the first point being $(R, \mu) = (1, 1)$ at yield and the second defined by the value of $R = R_{lim}$ “corresponding” to the ductility μ_{lim} defining the performance level. At any given period, both b and $\beta_{\theta d}$ tend to increase with ductility, therefore it is best to bias the fit by using a value of R_{lim} that is lower by about one half of the total dispersion (or roughly 15% for most cases) than what the median R - μ - T would assign to μ_{lim} ; otherwise, the importance of the more frequent low-intensity events would be over-represented, introducing unnecessary conservatism. Thus, let

$$b = \ln \mu_{lim} / \ln R_{lim}, \text{ for } R_{lim} = \max[1.0, 0.85R(\mu_{lim}, T)]. \quad (20)$$

The result is by definition 1.0 for structures deforming in the equal displacement range. Similarly, the value of $\beta_{\theta d}$ can be estimated at R_{lim} from the R - μ - T relationship.

5. EXAMPLE APPLICATION

As a simple case study, a four-story steel moment resisting frame is designed for the hazard of Figure 3. It has uniform story heights $h = 3.6\text{m}$, total height $H = 14.4\text{m}$ and beam spans (centreline dimensions) of $L = 9\text{m}$. Three distinct limit-states and corresponding performance levels are considered. For limiting damage in frequent low-intensity earthquakes, a strict serviceability (Immediate Occupancy, IO) interstory drift limit of $\theta_{lim} = 0.75\%$ is adopted, with a maximum allowable exceedance probability of 50% in 50yrs (practically the same as 10% in 10yrs). Akin to the design code basis, an ultimate limit-state (Life Safety, LS) level is set at a limiting ductility of 3.0 at 10% in 50yrs. Finally, to limit the chances of a global collapse, a Near Collapse (NC) limit-state is defined for $\mu = 4.5$ at 2% in 50yrs. As global ductility values are used in the above criteria, relative to an idealized system yield displacement, they will be quite lower than typical code values for R (or q), which reflect the presence of overstrength. In this example, overstrength is taken into account at the final step.

Definition of the three performance levels also requires choosing the magnitude of epistemic uncertainty and the confidence level for taking uncertainty into account for safety checking. In general, higher epistemic uncertainty values denote an increasing lack of knowledge in the actual structural demand and capacity for the limit state. Typically, model fidelity decreases with increasing inelastic response. Thus, epistemic uncertainty should be lower for elastic and nearly elastic response and increase with higher levels of inelastic deformation. Some rough guidance for choosing a dispersion value for the main damageable components may be found in pertinent literature. For example, Lignos and Krawinkler [35] report dispersions in the order of 30–40% for the ductility of beam plastic hinges at ultimate strength and final fracture. For consistency, we have assumed that the additional dispersion due to epistemic uncertainty, β_{USc} (or approximately $\beta_{U\theta}$), increases linearly with the logarithm of ductility, from a value of 0.20 at $\mu = 1$ to 0.35 at $\mu = 5$. Thus, overall epistemic

dispersions come out as 14%, 30% and 34% for IO, LS, and NC, respectively.

Considering the consequences of limit state violation, the confidence levels are set at 75% for the first two limit-states and 90% for NC. Note that a confidence level of 50% would ignore epistemic uncertainties completely. Typically a confidence level in the vicinity of 60% would be selected for IO performance for typical occupancies, where economic consequences rather than continuous operation is targeted. The selection of $x = 75\%$ for IO reflects a desire for improved performance at lower intensities. Similarly, the 90% confidence requirement for NC is meant to provide greater certainty that the structure will avoid collapse even at rare intensities, and is much stricter than typical code requirements.

Aschheim [11] suggests a simple way to estimate the yield drift for any story of a regular steel moment resisting frame as

$$\theta_y = \frac{\varepsilon_y}{6} \left(\frac{h}{d_{col} COF} + \frac{2L}{d_{bm}} \right), \quad (21)$$

where ε_y is the yield strain of steel, h the story height, L the beam span, COF the column overstrength factor and d_{col} , d_{bm} the column and beam depth, respectively. Let $\varepsilon_y = 0.21\%$ (for the expected strength of S355, or roughly 50ksi steel: $f_y = 1.2 \times 355 \text{MPa}$), $h = 3.6\text{m}$, $L = 9\text{m}$, $COF = 1.3$ (suggested values are 1.2 – 1.5), $d_{col} = 0.6\text{m}$, $d_{bm} = 0.70\text{m}$. Then, $\theta_y = 1.08\%$, and the limiting ductility for IO becomes $\mu_{limIO} = 0.75/1.08 = 0.70$. Design experience would typically suggest values of $\theta_y = 1\text{--}1.2\%$, confirming the above estimate. The corresponding roof drift ratio can be estimated if the drift profile over the height is known. Alternatively, an estimate of the coefficient of distortion a_{COD} may be used. As defined by Moehle [36], for a maximum interstory drift of θ_{max} , $a_{COD} \equiv \theta_{max}/(\delta_y/H)$. Herein, $a_{COD} = 1.25$ is adopted for this 4-story frame [37]. For a first-mode participation factor $\Gamma = 1.3$, the initial estimate of the ESDOF yield displacement is $\delta_y = \theta_y H / (\Gamma \cdot a_{COD}) = 0.095\text{m}$.

The system response is assumed to be approximately elastoplastic (since P-Delta effects do not dominate). Due to the different confidence levels employed, two YFS plots are generated, shown in Figure 9. The NC objective controls, requiring $C_y = 0.79$ versus 0.60 for IO. Perhaps it is not surprising that LS does not govern. For an assumed first-mode mass participation factor, $a_1 = 0.9$, the required base shear strength at yield is $F_y = 0.9(0.79)W = 0.71W$, which corresponds to the required strength of the system upon development of a mechanism (e.g. the strength observed in a first-mode pushover analysis). However, if a conventional design approach is used, the contribution of overstrength, Ω , can be considered to reduce the design strength. For a typical force-based design using nominal material properties and strength reduction factors, $\Omega \approx 2\text{--}3$. If, instead, design is based on a simple plastic collapse mechanism analysis using expected yield strengths, then overstrength appears due to some minor overproportioning (choosing slightly heavier sections), use of member centerline dimensions in the plastic mechanism analysis employed for design rather than true plastic hinge locations, and strain hardening. Values of overstrength on the order of $\Omega \approx 1.2\text{--}1.3$ are more reasonable in this case. Thus, the estimated value of C_y adjusted for overstrength should be on the order of 0.25 – 0.35 in the former case, and 0.55 – 0.60 in the latter. Sizing the structure accordingly would result with high fidelity in a frame that satisfies all performance objectives, as verified via Equation (1). This is expected for this regular low/mid-rise building, as estimates for θ_y , Γ , a_1 , a_{COD} and Ω are accurate. Some loss of fidelity may occur for structural configurations where height, plan or vertical irregularities, and the presence of higher modes may make such initial estimates less reliable. Then, nonlinear modeling of the initial design can offer improved estimates of such properties, allowing iterative refinements,

if needed. A comprehensive example of an eight-story frame appears in [38].

Since only a point estimate of yield drift θ_y was utilized, the sensitivity of the method to different choices is now considered. Table 1 shows the resulting C_y factors for $\theta_y = 0.9 - 1.3\%$, without consideration of overstrength. Aschheim and Black [13] identify the valley-shaped curves that define admissible design regions when using Yield Point Spectra. Similarly, an increase in δ_y will typically result in a decrease in required strength for limit states that are controlled by system ductility (in this case, the LS and NC objectives). Larger δ_y values also result in an increase in the required strength (and stiffness) for non-structural damage states defined in terms of displacement or drift demands in order to counter the increased flexibility. In this case, when coupled with the 75% confidence level, the associated C_y required for the IO objective increases substantially. The effect is so strong that it changes the governing limit-state: NC governs at or below $\theta_y = 1.2\%$ drift, while IO supersedes it for higher yield drift estimates. Still, unless one uses $\theta_y < 1.0\%$ or $\theta_y > 1.2\%$, the design C_y will not vary significantly. Considering all approximations involved, the end result, while not perfect, is reasonably close to fully satisfying all stated objectives.

Table 1: Yield strength coefficients of the ESDOF system for different values of the story yield drift. The LS and NC limit-states show sensitivity due to the change in the implied period (higher θ_y , longer T). For IO, the definition of the limit in terms of drift (rather than ductility) introduces larger changes. Analytical results lose accuracy for the NC limit-state, as it is close to dynamic instability.

Story yield drift, θ_y	ESDOF yield strength coefficient, C_y ^a		
	IO	LS	NC
0.9%	0.50 (0.50)	0.35 (0.36)	<u>0.90</u> (0.83)
1.0%	0.55 (0.55)	0.32 (0.33)	<u>0.84</u> (0.77)
1.1%	0.61 (0.60)	0.29 (0.30)	<u>0.78</u> (0.71)
1.2%	0.66 (0.66)	0.27 (0.28)	<u>0.73</u> (0.66)
1.3%	<u>0.72</u> (0.71)	0.25 (0.26)	0.69 (0.62)

^a numerical results are shown in normal font; analytical results are italicized, in parentheses; An underline indicates the controlling maximum C_y value for each row.

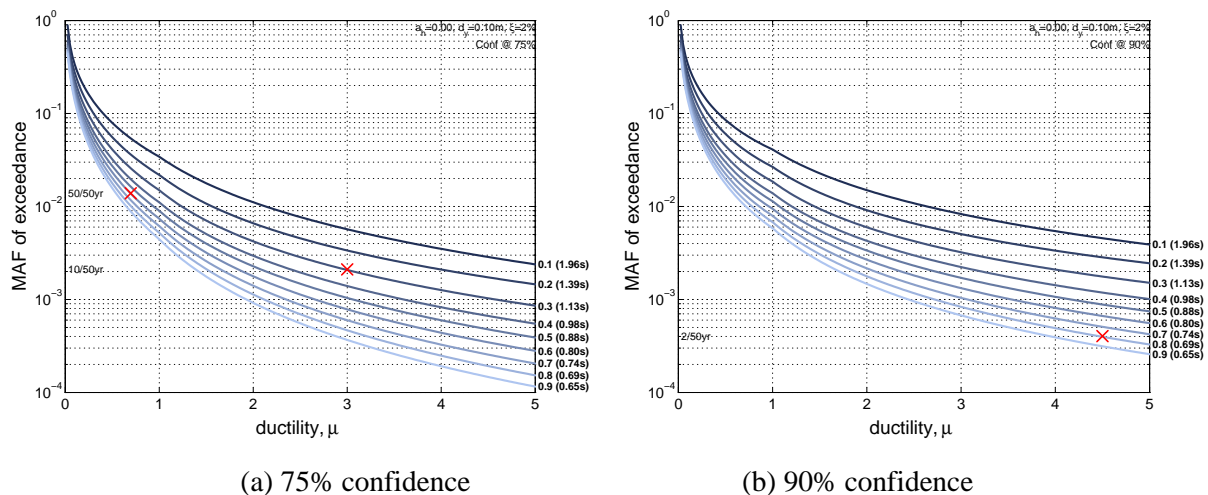


Figure 9. YFS contours determined for an elastoplastic system ($\delta_y = 0.095m$, $\xi = 2\%$) under the hazard of Figure 3. Two performance objectives ($\mu = 0.7$ and 3.0 at 50% and 10% in 50 yr, respectively) are determined at 75% confidence, while one ($\mu = 4.5$ at 2% in 50 yr) is set at a 90% level. The third objective governs with $C_y \approx 0.79$, corresponding to a period of $T \approx 0.7s$.

6. LIMITATIONS AND APPLICABILITY

The YFS approach, as delineated, incorporates four key approximations that will be reiterated to define its limits. First and foremost, an ESDOF is used to represent the MDOF system. Thus, optimal accuracy is achieved only for those structures where a static pushover analysis is capable of accurately estimating peak displacements. Plan asymmetric structures and tall buildings, where peak displacements and other response quantities may deviate from first mode estimates, may not be captured as accurately. Second, an assumed shape for the normalized force-deformation relationship and hysteretic characteristics of said ESDOF is needed. Thanks to the range of backbone shapes offered in SPO2IDA, the applicability of the YFS approach is not limited per se; the limitation mostly lies in the ability of the user to provide an accurate enough backbone shape for the system examined. Where prior information is lacking, an elastoplastic shape may be used initially, limiting the accuracy far from the yield point; subsequently, a more accurate shape may be deduced from a pushover analysis of the initial design. Third, in part due to the use of an ESDOF, $S_d(T_1)$ is employed as the IM, introducing unneeded conservatism at large ductilities [25]. Fourth, also as a consequence of the ESDOF, all performance objectives must be expressed in terms of the system global displacement (or ductility). Thus, some idea is needed of how local EDPs are distributed within the structure given the roof displacement. Earlier, this required information took the form of the COD to transform maximum interstory drift to roof drift. Ideally, such transformations should also provide the distribution of the resulting global displacement capacity, incorporating any uncertainty introduced by the transformation itself.

Such limitations, which are similar to (but less restrictive than) existing simplified approaches [12,24], do not restrict the applicability of the respective methods. Instead, they define the proper mode of application. Thus, unless our structure can be captured by an ESDOF and we have a good idea of what its backbone shape might look like, we cannot expect YFS to provide us with an accurate solution to this inverse problem in a single step. What it will provide, though, is a good starting point. Subsequent assessment and re-design iterations can be employed to reach the specified performance objectives with the desired accuracy. Each such cycle can inform the choice of backbone shape, yield displacement, local EDP profile, and even the effect of higher modes for an improved application of YFS in the next step. Alternatively, a user can opt to modify the MDOF design itself, performing iterations in this expanded parameter space. Either way, we suggest that the number of cycles to convergence will be reduced in comparison to existing simplified approaches.

7. CONCLUSIONS

Yield Frequency Spectra have been introduced as an intuitive and practical approach for preliminary or approximate performance-based seismic design. YFS extend Yield Point Spectra to account for hazard. In order to avoid an increase in dimensionality, YFS are plotted for a fixed value of yield displacement relevant to the design problem at hand, and illustrate the MAF of exceedance of the peak displacement or ductility response of SDOF oscillators having different strengths (or periods). Expressions provided herein, coupled with the use of YFS, provide a simple means to arrive at an accurate analytical solution that can accommodate site- and structure-specific characteristics, uncertainties, and desired confidence levels, considering one or more performance objectives, provided that these objectives can be related to the global displacement of an equivalent SDOF oscillator. Characteristic features of YFS are described along with analytical and numerical approaches for generating YFS. These

approaches are shown to generate results of similar fidelity in the case of an example.

Design philosophies have progressed from an emphasis on period of vibration in existing building codes to a recognition that yield drift ratios derive from kinematics and are relatively stable even as strength is tuned to satisfy specified performance objectives (and thereby influences stiffness and period). Thus, YFS are particularly useful for performance-based design approaches that exploit the relative stability of the yield displacement while accommodating a potentially large range of performance criteria. Using YFS, preliminary designs can be achieved that are very close to their performance targets. As a result, subsequent analysis and design cycles required to refine the preliminary design can be reduced or perhaps eliminated.

ACKNOWLEDGEMENTS

The first author gratefully acknowledges the support of the European Commission Research Executive Agency via Marie Curie grant PCIG09-GA-2011-293855.

REFERENCES

1. Cornell CA, Krawinkler H. Progress and challenges in seismic performance assessment. *PEER Center News* 2000; **3**(2), URL <http://peer.berkeley.edu/news/2000spring/index.html>, [Feb 2016].
2. fib. Probabilistic performance-based seismic design. *Bulletin 68*, International Federation of Structural Concrete, Lausanne, CH, 2012.
3. FEMA. Next-Generation Performance-Based Seismic Design Guidelines, Program Plan for New and Existing Buildings. *Report No. FEMA 445*, prepared for the Federal Emergency Management Agency, Washington, DC, 2006.
4. Krawinkler H, Zareian F, Medina RA, Ibarra LF. Decision support for conceptual performance-based design. *Earthquake Engineering and Structural Dynamics* 2006; **35**(1):115–133.
5. Mackie KR, Stojadinovic B. Performance-based seismic bridge design for damage and loss limit states. *Earthquake Engineering and Structural Dynamics* 2007; **36**:1953–1971.
6. Fragiadakis M, Papadrakakis M. Performance-based optimum seismic design of reinforced concrete structures. *Earthquake Engineering and Structural Dynamics* 2008; **37**:825–844.
7. Franchin P, Pinto P. Method for probabilistic displacement-based design of RC structures. *Journal of Structural Engineering* 2012; **138**(5):585–591.
8. Lazar N, Dolsek M. Risk-based seismic design - An alternative to current standards for earthquake-resistant design of buildings. *Proceedings of the 15th World Conference on Earthquake Engineering*, Lisbon, Portugal, 2012.
9. Fragiadakis M, Lagaros ND. An overview to structural seismic design optimisation frameworks. *Computers and Structures* 2011; **89**:1155–1165.
10. Priestley MJN. Performance based seismic design. *Bulletin of the New Zealand Society for Earthquake Engineering* 2000; **33**(3):325–346.
11. Aschheim M. Seismic design based on the yield displacement. *Earthquake Spectra* 2002; **18**(4):581–600.
12. Priestley MJN, Calvi GM, Kowalsky MJ. *Displacement-Based Seismic Design of Structures*. IUSS Press, Pavia, Italy, 2007.
13. Aschheim, M., and Black, E. Yield Point Spectra for Seismic Design and Rehabilitation. *Earthquake Spectra* 2000; **16**(2):317–335.
14. Vamvatsikos D, Cornell CA. Incremental Dynamic Analysis. *Earthquake Engineering and Structural Dynamics* 2002; **31**(3):491–514.
15. Cornell CA, Jalayer F, Hamburger RO, Foutch DA. The probabilistic basis for the 2000 SAC/FEMA steel moment frame guidelines. *Journal of Structural Engineering* 2002; **128**(4):526–533.
16. Jalayer F. Direct probabilistic seismic analysis: Implementing non-linear dynamic assessments.

- PhD Dissertation*, Department of Civil and Environmental Engineering, Stanford University, Stanford, CA, 2003.
17. Vamvatsikos D, Cornell CA. Applied Incremental Dynamic Analysis. *Earthquake Spectra* 2004; **20**(2):523–553.
 18. FEMA. Quantification of Building Seismic Performance Factors. *Report No. FEMA P695*, prepared for the Federal Emergency Management Agency, Washington, DC, 2009.
 19. Bradley B. A comparison of intensity-based demand distributions and the seismic demand hazard for seismic performance assessment. *Earthquake Engineering and Structural Dynamics* 2013; **42**:2235–2253.
 20. Vamvatsikos D. Derivation of new SAC/FEMA performance evaluation solutions with second-order hazard approximation. *Earthquake Engineering and Structural Dynamics* 2013; **42**(8): 1171–1188.
 21. Inoue T, Cornell CA. Seismic hazard analysis of multi-degree-of-freedom structures. *Report RMS-08*, Reliability of Marine Structures Program, Stanford University, Stanford, CA, 1990.
 22. Bazzurro P, Cornell, CA. Seismic hazard analysis of nonlinear structures. II: Applications. *Journal of Structural Engineering* 1994; **120**(11):3345–3365.
 23. Ruiz-Garcia J, Miranda E. Probabilistic estimation of maximum inelastic displacement demands for performance-based design. *Earthquake Engineering and Structural Dynamics* 2007; **36**:1235–1254.
 24. IBC. *2012 International Building Code*. International Code Council, IL, USA, 2011.
 25. Luco N, Bazzurro P. Does amplitude scaling of ground motion records result in biased nonlinear structural drift responses? *Earthquake Engineering and Structural Dynamics* 2007; **36**:1813–1835.
 26. Haselton CB, Baker JW, Liel AB, Deierlein GG. Accounting for ground-motion spectral shape characteristics in structural collapse assessment through an adjustment for epsilon. *Journal of Structural Engineering ASCE* 2011; **137**(3):332–344.
 27. Miranda E. Estimation of inelastic deformation demands of SDOF systems. *Journal of Structural Engineering ASCE* 2001; **127**(9):1005–1012.
 28. SAC/FEMA. Recommended seismic design criteria for new steel moment-frame buildings. FEMA-350, SAC Joint Venture, Federal Emergency Management Agency, Washington DC.
 29. Vamvatsikos D, Cornell CA. Direct estimation of the seismic demand and capacity of oscillators with multi-linear static pushovers through Incremental Dynamic Analysis. *Earthquake Engineering and Structural Dynamics* 2006; **35**(9): 1097–1117.
 30. Miranda E. Evaluation of site-dependent inelastic seismic design spectra. *Journal of Structural Engineering ASCE* 1993; **119**(5):1319–1338.
 31. Baker JW, Cornell CA. A vector-valued ground motion intensity measure consisting of spectral acceleration and epsilon. *Earthquake Engineering and Structural Dynamics* 2005; **34**:1193–1217.
 32. Hatzigeorgiou GD. Damping modification factors for SDOF systems subjected to near-fault, far-fault and artificial earthquakes. *Earthquake Engineering and Structural Dynamics* 2010; **39**:1239–1258.
 33. Vamvatsikos D, Aschheim M. *YFSapp: Yield Frequency Spectra application tool*. URL <http://users.ntua.gr/divamva/software/YFSapp.xls> [accessed 23/Sep/2015].
 34. Vamvatsikos D. Accurate application and second-order improvement of the SAC/FEMA probabilistic formats for seismic performance assessment. *Journal of Structural Engineering ASCE* 2014; **140**(2): 04013058.
 35. Lignos DG and Krawinkler H. Deterioration modeling of steel components in support of collapse prediction of steel moment frames under earthquake loading. *Journal of Structural Engineering ASCE* 2011; **137**(11): 1291–1302.
 36. Moehle JP. Displacement-based design of RC structures subject to earthquakes. *Earthquake Spectra* 1992; **8**(3): 403–428.
 37. Gupta A, Krawinkler K. Estimation of seismic drift demands for frame structures. *Earthquake Engineering and Structural Dynamics* 2003; **29**:1287–1305.
 38. Vamvatsikos D, Katsanos EI, Aschheim MA. A case study in performance-based design using yield frequency spectra. *Proceedings of the SECED 2015 Conference*, Cambridge, UK, 2015.